Molecular dynamics simulations of Cl^+ etching on a Si(100) surface

F. Gou, E. Neyts, M. Eckert, S. Tinck, and A. Bogaerts[a)]
Department of Chemistry, Research Group PLASMANT, University of Antwerp, Universiteitsplein 1, B-2610 Wilrijk-Antwerp, Belgium

(Received 14 December 2009; accepted 14 February 2010; published online 3 June 2010)

Molecular dynamics simulations using improved Tersoff–Brenner potential parameters were performed to investigate Cl^+ etching of a $\{2\times1\}$ reconstructed Si(100) surface. Steady-state Si etching accompanying the Cl coverage of the surface is observed. Furthermore, a steady-state chlorinated reaction layer is formed. The thickness of this reaction layer is found to increase with increasing energy. The stoichiometry of $SiCl_x$ species in the reaction layer is found to be $SiCl:SiCl_2:SiCl_3=1.0:0.14:0.008$ at 50 eV. These results are in excellent agreement with available experimental data. While elemental Si products are created by physical sputtering, most $SiCl_x$ $(0<x<4)$ etch products are produced by chemical-enhanced physical sputtering. © *2010 American Institute of Physics*. [doi:10.1063/1.3361038]

I. INTRODUCTION

Chlorine-based plasma-assisted etching processes play an important role in the fabrication of ultralarge-scale circuits.[1–8] During etching, ions and radicals originating from the Cl_2 plasma impinge on the surface and cause removal of atoms from the surface.[9,10] It is well known that the energy of ions impinging on the silicon surface has a decisive effect on etching.[11–18] In order to obtain insight into the etching mechanisms occurring on surfaces, many experiments have been designed to investigate the plasma-surface interactions.[5,6,16,19–21] However, due to the enormous complexity of the plasma environment and the lack of *in situ* characterization of surfaces in etching plasmas, etching mechanisms are still not completely understood.

In the past decades, molecular dynamics (MD) simulations have been applied to help visualize the evolving surface morphology, surface composition, and etching products to gain a deeper understanding of the etch process.[22–34] Ohta and Hamaguchi[33] developed Stillinger–Weber (SW) type potential sets for the Si–Cl system, based on *ab initio* quantum mechanical calculations. They also performed MD simulations to investigate Si reactive ion etching by Cl^+. Their simulation results showed that etch rates were in good agreement with experimental data. Barone and Graves[35] also used the SW potentials to investigate etching mechanisms of silicon by chlorine. Their results show that physical sputtering is the most important etch mechanism, but chemical sputtering and direct abstractive etching mechanisms are also important in the energy range from 10 to 50 eV. Feil *et al.*[24] performed MD simulations of Cl_2 interacting with Si using SW potentials. They found a reaction layer consisting of $SiCl_2$ and $SiCl_3$ groups. They also discussed the dependence of chemical sputtering on the roughness formation of chlorined silicon surfaces during ion bombardment. They suggested that the chlorine passivation of the Si surface results in the roughness due to the high activation barrier for surface diffusion.

In the present study, we examine energetic Cl^+ ions interacting with a silicon surface. In the past, many MD simulations have been performed to investigate Cl^+ etching silicon surfaces using SW potentials.[23,24,27,28] However, it is stated in Ref. 30 that SW potentials are too repulsive, such that they are unable to predict spontaneous etching at room temperature.[30] In order to overcome this disadvantage, Humbird and Graves[36] developed a Tersoff–Brenner type potential for the Si–Cl system and successfully predicted thermal Cl spontaneous etching of Si.[30]

Experimental results indicate that the reaction layer formed near the surface region during etching plays an important role in etching.[37,38] However, for Cl^+ etching of Si, no MD simulations using the improved Tersoff–Brenner type potentials have been performed yet with the aim of investigating the properties of the reaction layer and elucidating its role in the etching process. In this study, the improved Tersoff–Brenner potential is applied for the simulation of Cl^+ etching on Si(100) surfaces. We examine the formation and the composition of the reaction layer in detail and compare with some experimental data. The purpose is to provide a closer insight into the chemical and physical processes that occur on the surface during Cl^+ etching of a silicon surface.

II. SIMULATION DETAILS

MD simulations are utilized to investigate the behavior of incident Cl^+ interacting with a silicon surface. In classical MD simulations particles are treated purely classically and no quantum effects are considered. The motion of all movable atoms is determined by integrating Newton's equations of motion. In the present simulations, impacts of Cl atoms are considered, i.e., the assumption is made that when Cl^+ ions approach the silicon surface, they are neutralized through an Auger process occurring before the ions interact strongly with the surface atoms.

To obtain a reconstructed Si(100) 2×1 surface of the single crystal, we started with a bulk crystalline silicon simulation cell holding 3000 atoms. The topmost layer contains 50 Si atoms (defined as 1 monolayer, ML) and has a surface area of about 738.21 $Å^2$. Periodic boundary conditions were

a)Electronic address: annemie.bogaerts@ua.ac.be.

applied along the x- and y-directions (parallel to the surface plane). Atoms of the two bottom-most layers were fixed in order to anchor the simulation cell. All other atoms are movable under external forces derived from the interatomic potential.

Cl^+ bombarding a silicon surface is modeled as a series of individual atoms interacting sequentially with the surface. At the start of each trajectory, a Cl atom is randomly placed above the surface. The height above the surface is beyond the cutoff of the potential. The velocity-Verlet integration scheme with a fixed time step was implemented.[39] A time step of 0.5 fs was used for all simulations. The total integration time for tracking each trajectory was 1.0 ps. Within each trajectory, when incident Cl atoms begin to interact with the surface, the temperature of the sample rapidly increases. After 0.6 ps interacting with the sample, the Berendsen[40] heat bath with a coupling constant of 0.01 ps was applied to maintain the sample at a constant temperature of 300 K. There was no relaxation interval between two sequential bombardments. Ion energies ranging from 25 to 150 eV are chosen with normal incident angle.

According to first order desorption theory definition, a cluster is considered to thermally desorb from the surface and form an etch product when the cluster's binding energy with the surface is smaller than a certain threshold energy. Species matching this criterion are searched and removed from the simulation at the end of each trajectory. This process is defined as chemical etching. The threshold energy can be obtained from[22,41]

$$E_b = k_b T \ln(\tau A), \quad (1)$$

where k_b is the Boltzmann constant, T is the surface temperature, τ is a time constant, which is smaller than the real time that elapses before a subsequent molecule impacts, and A is a constant. In the current simulations, the values of τ and A are 1 μs and 10^{12} s^{-1}.[22]

III. RESULTS AND DISCUSSION

A. Initial verification of the model

Before studying the etch process in detail, we need to verify the reliability of our model. Therefore, it is necessary to compare our simulation results with some available experimental and other simulation data. Figure 1 shows the calculated Si etch yield (per incident Cl) as a function of ion energy, along with MD simulation data performed by Hanson *et al.*[28] using the SW potential and experimental values from Balooch *et al.*[42] and Chang and Sawin.[43] It is noted that at lower energies our MD simulation results using the Tersoff–Brenner potential are in good agreement with the MD data of Hanson, as well as with the experimental values.

Compared with Hanson's simulations, our model is improved on two aspects: (1) the empirical potential and (2) the thermal desorption process. Indeed, the Tersoff–Brenner potential employed in the current simulations has many advantages over the SW potential used by Hanson. In the Tersoff–Brenner potential, the effects of the type and the number of neighbors for each Si atom on the Si–Si bond strength are considered. Humbird's simulation results show that the

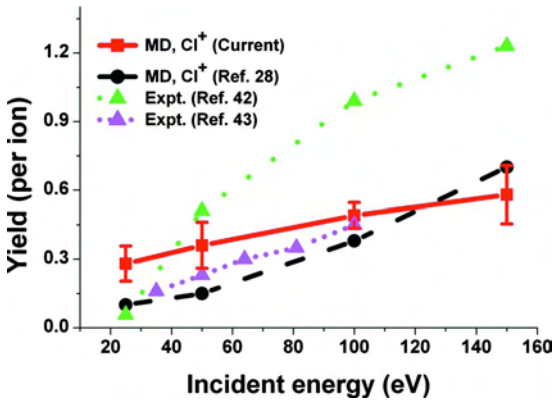

FIG. 1. (Color online) Etch yields (number of Si atoms removed per incident ion) as a function of incident energy. Besides the present calculation results, also experimental data (Refs. 42 and 43) and the results of other MD simulations (Ref. 28) are presented. The error bars are calcuated as the standard deviation corresponding to a normal distribution of the performed simulations.

Tersoff–Brenner potential can indeed predict Cl spontaneous etching. However, the SW potential cannot predict this.[30] In addition, both SW and Tersoff–Brenner potentials cannot model a screened Coloumb interaction between two atoms. To overcome this deficiency, in the present simulations, the Molière-type repulsive screened Coloumb potential is included at short separations of 0.8 Å for the Si–Cl pair.[36] Concerning the second improvement, in Hanson's model thermal desorption between two sequential impacts is absent. In our model, a simple first order thermal desorption model was used to predict whether a molecule could desorb between two impacts.

It is noted in Fig. 1 that with increasing incident energy the discrepancy between both MD results and the experimental data obtained by Balooch *et al.*[42] increases. This increasing discrepancy may still be due to the simple empirical potential and incident species. Indeed, a potential intended for the simulation of particle bombardment on surfaces needs to take into account accumulation of bulk and surface defects by penetrating ions. However, in our present Tersoff–Brenner potential these aspects are absent. Therefore, the Tersoff–Brenner potential for the Si–Cl system could still be improved in this respect. In addition, Balooch *et al.* used a monoenergetic beam of chlorine ions in which both Cl^+ and Cl_2^+ were present. In order to compare with their simulation yield data, Hanson *et al.* calibrated the yield data. However, most of the difference between the simulation and experimental data remained. On the other hand, both simulation results agree well with the experimental data obtained by Chang and Sawin[43] using a pure Cl^+ ion beam. Hence, the Tersoff–Brenner potential is suitable to predict the behavior of the Si–Cl system during Si etching by Cl^+.

B. Study of Cl^+ adsorption on the Si surface

When the Cl^+ ions interact with the Si surface, they begin to lose their kinetic energy to the lattice through collisions.[44] Cl^+ ions may be adsorbed on the surface or scatter away from the surface. In order to examine the uptake of incident Cl^+ ions on the surface, the number of Cl atoms

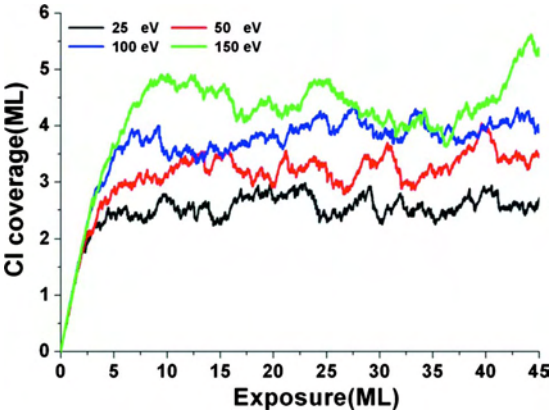

FIG. 2. (Color online) Calculated Cl coverage as a function of exposure for the four energies under study (25, 50, 100, and 150 eV) at 300 K. Here 1 ML exposure is equivalent to 50 surface atoms.

adsorbed on the surface is shown in Fig. 2 as a function of the number of incident Cl atoms for four different energies (25, 50, 100, and 150 eV). During the initial stage up to about 5 ML of exposure, the uptake of Cl atoms sharply increases and the coverages for the four energies are almost equivalent. When the simulation proceeds, a saturated coverage is observed. The steady-state coverage of Cl atoms increases with incident energy.

Due to the uptake of Cl atoms on the surface and the removal of Si atoms from the surface, the surface structure is modified. Figure 3 shows the calculated depth profiles of the modified Si surfaces at 25, 50, 100, and 150 eV after exposure to 45 ML of Cl, respectively. Note that the depth profile is obtained by averaging over the lateral dimension of the sample. The density of crystalline Si is about 0.05 atoms/Å^3. Regardless of the incident energy, after bombardment with Cl atoms, a chlorined reaction layer is formed near the surface region. A density gradient of Si through the reaction layer is observed. This is due to Si etching. Here, the reaction layer is referred to the region where Cl atoms appear. The thickness of the reaction layer increases with incident energy. With increasing incident energy, more Cl atoms can penetrate deeper into the bulk. At 25 eV the ratio of Cl to Si in the near-surface region is close to 1. At higher energies, especially greater than 100 eV, the ratio of Cl to Si in the near-surface region is less than 1.

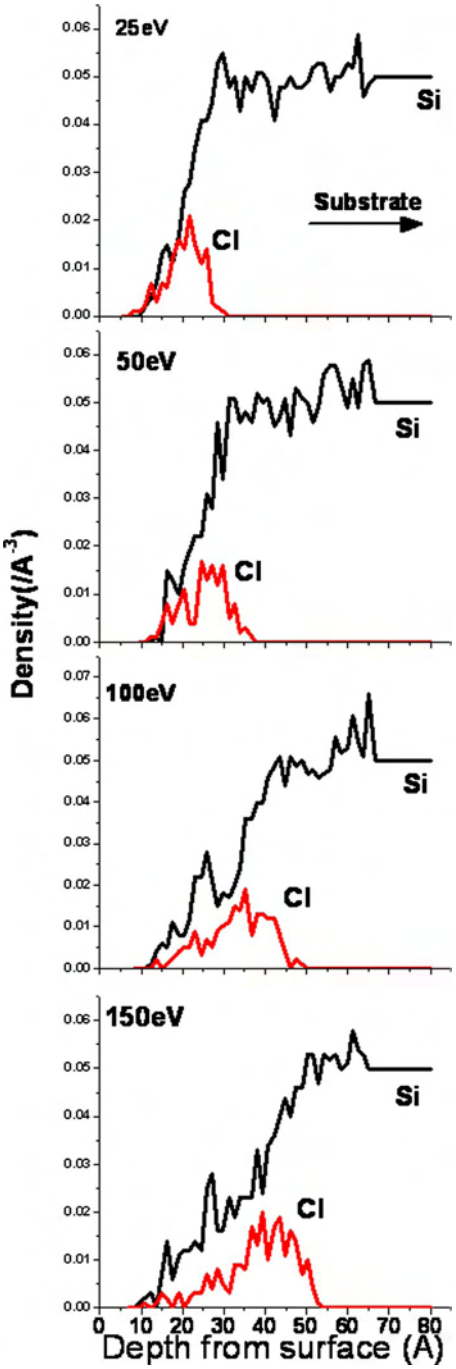

FIG. 3. (Color online) Calculated depth profiles of the modified Si surfaces at 25, 50, 100, and 150 eV after an exposure of 45 ML of Cl atoms. The depth profiles are obtained by averaging over the lateral dimension of the sample, with a depth resolution of 1.3575 Å.

C. Formation of $SiCl_x$ species in the surface reaction layer

When Cl atoms deposit on Si, they will react with Si atoms with dangling bonds to form Si–Cl bonds because the latter are energetically more favorable than Si–Si bonds. Figure 4(a) shows the relative fractions of SiCl, $SiCl_2$, and $SiCl_3$ species in the reaction layer after exposure to 45 ML of Cl atoms as a function of ion energy. Here, the relative fraction is defined as the ratio of the number of $SiCl_x$ ($x=1-3$) to the total number of SiCl, $SiCl_2$, and $SiCl_3$. In the present simulations, a simple first order thermal desorption model was employed. Therefore, once $SiCl_4$ species were formed on the surface between two sequential impacts, they were removed from the substrate as etching products. Hence, no $SiCl_4$ species are found on the surface. For all energy cases, SiCl species are clearly dominant, followed by $SiCl_2$ and $SiCl_3$.

Figure 4(b) shows the time evolution of $SiCl_x$ species in the reaction layer at Cl^+ ion bombardment energy of 150 eV. During the initial stage ranging from 0 to 10 ML, the fraction of SiCl decreases while the fraction of $SiCl_2$ increases with increasing Cl exposure. In comparison with Fig. 2, we observe that the relative fractions of $SiCl_x$ species reach a steady-state after the Cl coverage reaches saturation values. After about 40 ML of Cl exposure, the fraction of SiCl species again decreases slightly and the $SiCl_2$ fraction increases.

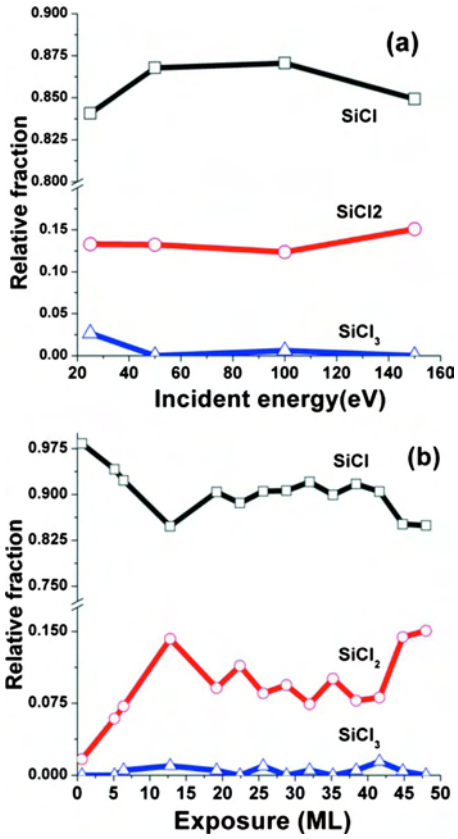

FIG. 4. (Color online) Calculated relative fractions of SiCl, $SiCl_2$, and $SiCl_3$ species in the reaction layer (a) as a function of incident energy after exposure to 45 ML of Cl atoms and (b) as a function of exposure with Cl atoms of 150 eV.

Figures 5(a) and 5(b) show the depth profiles of SiCl and $SiCl_2$ species in the reaction layer after exposure to 45 ML of Cl atoms at 25 and 150 eV, respectively. Since the fraction of $SiCl_3$ species in the reaction layer is very small, its depth profile is not shown. It is noted that SiCl is the predominant

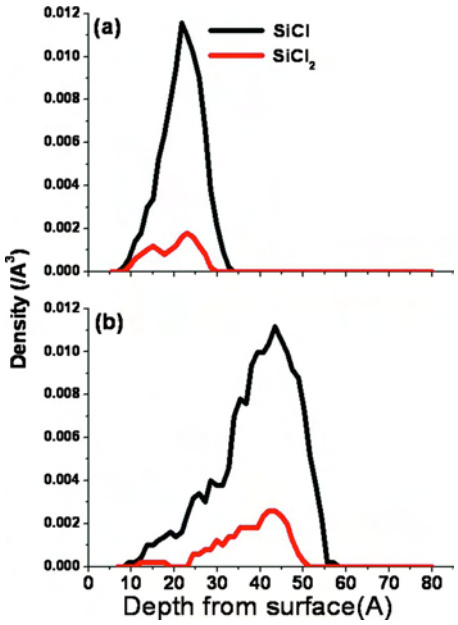

FIG. 5. (Color online) Calculated depth profiles of SiCl and $SiCl_2$ species in the reaction layer after 45 ML of Cl exposure at (a) 25 eV and (b) 150 eV.

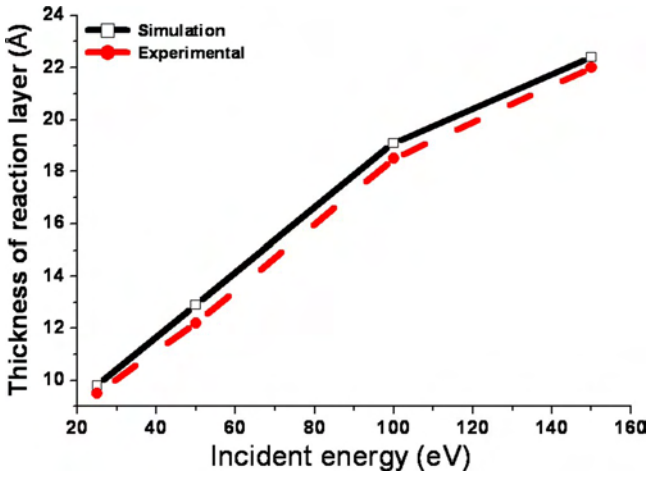

FIG. 6. (Color online) Calculated thicknesses of the reaction layer as a function of incident energy after 45 ML of Cl exposure, in comparison with experimental data (Ref. 21) Note that the thickness is calculated from full width at half maximum.

species throughout the reaction layer. For the 25 eV case, shown in Fig. 5(a), SiCl and $SiCl_2$ are mostly confined to the top ~30 Å. The SiCl concentration peaks at 21 Å below the surface; while $SiCl_2$ species almost persist to a depth of ~23 Å. At 150 eV shown in Fig. 5(b), it is observed that near the surface almost no $SiCl_2$ species exist, and the concentrations of SiCl and $SiCl_2$ species peak at ~45 Å below the surface.

Many experiments and simulations have been performed to investigate the reaction layer. Herman *et al.*[45] studied Cl_2 plasma etching of Si(100) using laser desorption-laser induced fluorescence and x-ray photoelectron spectroscopy (XPS). They found that a steady-state reaction layer was quickly formed after exposure to the Cl_2 plasma. This behavior is observed in our current simulations as well. Indeed, in our simulations, a steady-state chemical composition in the reaction layer is noticed after several ML of Cl exposure. Layadi *et al.*[5] measured the thickness of the reaction layer during the Cl_2 plasma etching of Si(100) using XPS. Figure 6 shows results of their experiment and our current simulation results as a function of incident energy. Note that for the simulation data, the film thickness is defined as full width at half maximum. Furthermore, in the experiment by Layadi *et al.*, the reaction layer was produced by a plasma, i.e., consisting of a high flux of thermalized Cl radicals (and Cl_2 molecules) besides Cl^+ ions, whereas in the simulations only monoenergetic Cl atoms were considered. Hence, this comparison holds only true when assuming that the thickness of the reaction layer is determined by the ion energies. With increasing incident energy, the thickness of the reaction layer increases. It is noted that the simulation results are in excellent agreement with the experimental data. Furthermore, from the XPS measurements, Layadi and Lee *et al.*[5] also found that the reaction layer consisted of SiCl, $SiCl_2$, and $SiCl_3$ components. No $SiCl_4$ was detected.

MDs simulations by Feil and co-workers also predicted the modified surface structure with $SiCl_2$ and $SiCl_3$ groups. The presence of $SiCl_x$ ($x<4$) in the layer is in good agreement with our present simulation results. Their analysis

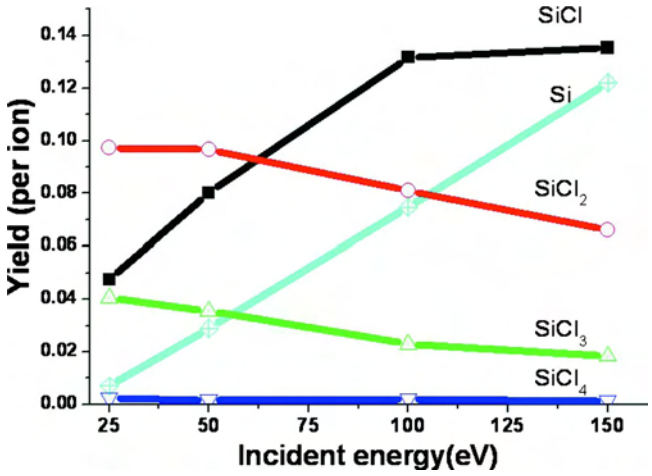

FIG. 7. (Color online) Calculated product yields of $SiCl_x$ (x=0–4) species as a function of incident energy after 45 ML of Cl exposure.

shows that the stoichiometry of the $SiCl_x$ species in the reaction layer at 50 eV was $SiCl:SiCl_2:SiCl_3 = 1.0:0.14:0.008$. When averaging our steady-state data for the $SiCl_x$ species at 50 eV, we obtain a stoichiometry of $SiCl:SiCl_2:SiCl_3$ equal to 1.0:0.12:0.005. Comparison shows that our simulation results are in excellent agreement with their experimental data.

D. Product yields of $SiCl_x$ species

During the bombardment with energetic Cl atoms, some Cl atoms adsorb on the surface and some are incorporated into the Si bulk by forming Si–Cl bonds. When the simulation proceeds, weakly bound $SiCl_x$ species are formed in the reaction layer. Volatile $SiCl_x$ (x=1–4) groups are created. These weakly bound species may be ejected by cascaded collisions or thermally desorb from the surface. The product yields of $SiCl_x$ (x=0–4) as a function of incident energy are presented in Fig. 7 after exposure to 45 ML of Cl. At energies below about 60 eV, $SiCl_2$ products are dominant; when the incident energy is greater than 60 eV, SiCl products become dominant. For all energies, the yield of $SiCl_4$ products is the smallest. The yield of elemental Si products increases with incident energy and becomes almost equal to the SiCl product yield at 150 eV. Indeed, elemental Si can only be ejected by physical sputtering, and this process becomes more important at higher ion energies. The SiCl yield increases with increasing incident energy from 25 to 100 eV and it stays more or less constant for higher energies. Finally, the yields of the $SiCl_x$ (x=2–4) etch products decrease with incident energy. From these results, we can obtain more insight in the relative importance of the various etching mechanisms, as will be discussed below.

E. Relative importance of different etching mechanisms

Based on previous experimental and modeling results, three etching mechanisms have been proposed in the literature.[8] When an energetic particle bombards a silicon surface, products leaving the surface within ~1 ps arise due to momentum transfer during collisions; this is called "physical sputtering." Among the sputtered products, no incident reactive atoms (F, Cl, etc.) are present. When Cl^+ ions impact on the silicon surface, silicon atoms near the surface region may be sputtered as a direct result of momentum transfer. Therefore, in Fig. 7, the yield of Si atoms is completely attributed to pure physical sputtering.

Second, pure "chemical etching" is defined as the process in which products that are weakly bound with the surface thermally desorb. With energetic Cl^+ ions bombarding the Si surface, some Si–Si bonds may break to form dangling bonds. Adsorbed Cl atoms chemically react with the Si on the surface to form volatile species (like $SiCl_x$ (x=1–3) as shown in Fig. 4) that are still weakly bound to the sample. In fact, these weakly bound volatile species may thermally desorb from the surface. The process takes place on a long time scale (maybe ms) and results from relaxation of the chemical bonds. Therefore, the MD method is unable to reproduce long time scale thermal desorption. To overcome this limitation, we adapted in our simulations the first order thermal desorption model presented by Barone and Graves[41] to determine whether these weakly bound species can thermally desorb from the surface. At the end of each trajectory, weakly bound species are checked. If the binding energy between the atoms of a certain species and the surface atoms is smaller than E_b (as obtained from Eq. (1) above), it is assumed that the species will thermally desorbed from the surface before the next trajectory.

Considering the third etching mechanism, when sputtered species leave the surface due to collisions but the emitted products consist of previously deposited chemically reactive atoms, the process is defined as "chemical-enhanced physical sputtering."[8] Hence, when an energetic Cl^+ ion impacts the Si surface, the weakly bound species on the surface created previously may be sputtered physically away from the surface within ~1 ps. According to the above definitions, the yields of the $SiCl_x$ products shown in Fig. 7 are attributed to either pure chemical etching or chemical-enhanced physical sputtering.

Figure 8 shows the relative ratios of the number of SiCl, $SiCl_2$, and $SiCl_3$ etch products by chemical etching to the number of these species produced by chemical-enhanced physical sputtering as a function of Cl incident energy. It is noted that the ratio contributing to produce $SiCl_x$ species by chemical etching is less than 50%. Therefore, it can be concluded that most products originate from chemical-enhanced physical sputtering.

IV. CONCLUSION

We performed MDs simulations of Cl^+ etching on a Si(100) surface with energies of 25, 50, 100, and 150 eV. For all energies it is found that almost all incident Cl atoms deposit on the surface before an exposure of 5 ML. Subsequently, saturation behavior of the Cl coverage on the surface is observed. At the same time, a steady-state etching is reached and a steady-state reaction layer near the surface region is created. In the reaction layer, there exist $SiCl_x$ (x<4) components, which is also observed in the experimental data of Layadi and Lee *et al.* The stoichiometry of SiCl,

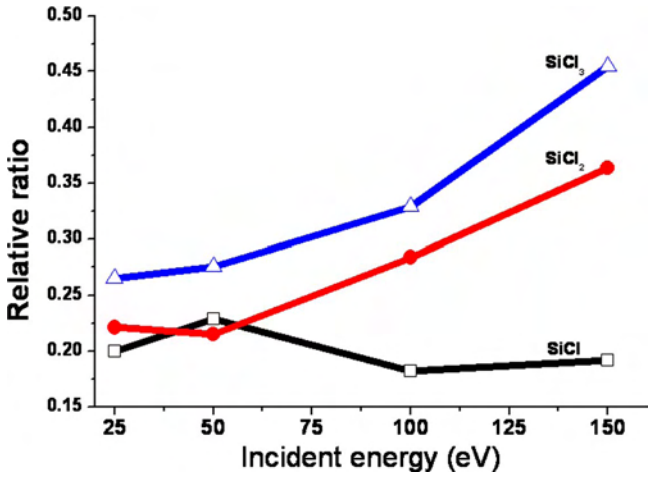

FIG. 8. (Color online) Calculated relative ratios as a function of Cl incident energy. Here the relative ratio is defined as the ratio of the number of SiCl, $SiCl_2$, and $SiCl_3$ species produced by chemical etching to the number of SiCl, $SiCl_2$, and $SiCl_3$ species produced by chemical-enhanced physical sputtering.

$SiCl_2$, and $SiCl_3$ is calculated as 1.0, 0.12, and 0.005 which is in excellent agreement with experimental values and other simulation results. Our simulated thickness of the reaction layer is also in excellent agreement with experimental data. The product yields of $SiCl_x$ $(x=0-4)$ are also predicted. Elemental Si products are created by pure physical sputtering. The dominant etch products SiCl and $SiCl_2$ are formed due to chemical-enhanced physical sputtering.

ACKNOWLEDGMENTS

F. Gou and E. Neyts are indebted to the Fund for Scientific Research (FWO) Flanders for financial support. M. Eckert and S. Tinck acknowledge the Institute for the Promotion of Innovation by Science and Technology in Flanders (IWT Flanders) for financial support. The authors also thank IMEC for financial support as well as the CalcUA computing facilities of the University of Antwerp.

[1]S. Tinck, W. Boullart, and A. Bogaerts, J. Phys. D **42**, 095204 (2009).
[2]C. M. Aldao, A. Agrawal, R. E. Butera, and J. H. Weaver, Phys. Rev. B **79**, 125303 (2009).
[3]M. Armacost, P. D. Hoh, R. Wise, W. Yan, J. J. Brown, J. H. Keller, G. A. Kaplita, S. D. Halle, K. P. Muller, M. D. Naeem, S. Srinivasan, H. Y. Ng, M. Gutsche, A. Gutmann, and B. Spuler, IBM J. Res. Dev. **43**, 39 (1999).
[4]G. Cunge, M. Mori, M. Kogelschatz, and N. Sadeghi, Appl. Phys. Lett. **88**, 051501 (2006).
[5]N. Layadi, V. M. Donnelly, and J. T. C. Lee, J. Appl. Phys. **81**, 6738 (1997).
[6]N. Layadi, V. M. Donnelly, J. T. C. Lee, and F. P. Klemens, J. Vac. Sci. Technol. A **15**, 604 (1997).
[7]I. W. Rangelow, Surf. Coat. Technol. **97**, 140 (1997).
[8]H. F. Winters and J. W. Coburn, Surf. Sci. Rep. **14**, 162 (1992).
[9]E. S. Aydil and D. J. Economou, J. Electrochem. Soc. **139**, 1396 (1992).
[10]A. Manenschijn, E. Vanderdrift, G. C. A. M. Janssen, and S. Radelaar, J. Appl. Phys. **69**, 7996 (1991).
[11]P. K. Charvat, E. E. Krueger, and A. L. Ruoff, J. Vac. Sci. Technol. B **4**, 812 (1986).
[12]E. Ikawa and Y. Kurogi, Jpn. J. Appl. Phys., Part 1 **22**, 1263 (1983).
[13]A. W. Kolfschoten, R. A. Haring, A. Haring, and A. E. Devries, J. Appl. Phys. **55**, 3813 (1984).
[14]J. S. Lechaton and J. L. Mauer, J. Electrochem. Soc. **127**, C88 (1980).
[15]Y. Osano and K. Ono, Jpn. J. Appl. Phys., Part 1 **44**, 8650 (2005).
[16]S. D. Park, D. H. Lee, and G. Y. Yeom, J. Korean Phys. Soc. **47**, 469 (2005).
[17]S. D. Park, D. H. Lee, and G. Y. Yeom, Electrochem. Solid-State Lett. **8**, C106 (2005).
[18]F. H. M. Sanders, A. W. Kolfschoten, J. Dieleman, R. A. Haring, A. Haring, and A. E. Devries, J. Vac. Sci. Technol. A **2**, 487 (1984).
[19]I. Bello, W. H. Chang, and W. M. Lau, J. Appl. Phys. **75**, 3092 (1994).
[20]J. D. Casey, A. F. Doyle, R. G. Lee, D. K. Stewart, and H. Zimmermann, Microelectron. Eng. **24**, 43 (1994).
[21]J. W. Coburn, J. Vac. Sci. Technol. B **12**, 1384 (1994).
[22]C. F. Abrams and D. B. Graves, J. Appl. Phys. **86**, 5938 (1999).
[23]M. E. Barone, T. O. Robinson, and D. B. Graves, IEEE Trans. Plasma Sci. **24**, 77 (1996).
[24]H. Feil, J. Dieleman, and B. J. Garrison, J. Appl. Phys. **74**, 1303 (1993).
[25]F. Gou, L.Z. T. Chen, C. Meng, and Q. Qian, Appl. Phys. A: Mater. Sci. Process. **88**, 385 (2007).
[26]F. Gou, A. W. Kleyn, and M. A. Gleeson, Int. Rev. Phys. Chem. **27**, 229 (2008).
[27]D. E. Hanson, J. D. Kress, and A. F. Voter, J. Vac. Sci. Technol. A **17**, 1510 (1999).
[28]D. E. Hanson, A. F. Voter, and J. D. Kress, J. Appl. Phys. **82**, 3552 (1997).
[29]D. Humbird and D. B. Graves, Plasma Sources Sci. Technol. **13**, 548 (2004).
[30]D. Humbird and D. B. Graves, J. Appl. Phys. **96**, 791 (2004).
[31]A. Iwakawa, T. Nagaoka, H. Ohta, K. Eriguchi, and K. Ono, Jpn. J. Appl. Phys. **47**, 8560 (2008).
[32]N. A. Kubota, D. J. Economou, and S. J. Plimpton, J. Appl. Phys. **83**, 4055 (1998).
[33]H. Ohta and S. Hamaguchi, J. Vac. Sci. Technol. A **19**, 2373 (2001).
[34]S. Rauf, T. Sparks, P. L. G. Ventzek, V. V. Smirnov, A. V. Stengach, K. G. Gaynullin, and V. A. Pavlovsky, J. Appl. Phys. **101**, 033308 (2007).
[35]M. E. Barone and D. B. Graves, J. Appl. Phys. **78**, 6604 (1995).
[36]D. Humbird and D. B. Graves, J. Chem. Phys. **120**, 2405 (2004).
[37]G. S. Oehrlein, J. Vac. Sci. Technol. A **11**, 34 (1993).
[38]T. E. F. M. Standaert, M. Schaepkens, N. R. Rueger, P. G. M. Sebel, G. S. Oehrlein, and J. M. Cook, J. Vac. Sci. Technol. A **16**, 239 (1998).
[39]L. Verlet, Phys. Rev. **159**, 98 (1967).
[40]H. J. C. Berendsen, J. P. M. Postma, W. F. Vangunsteren, A. Dinola, and J. R. Haak, J. Chem. Phys. **81**, 3684 (1984).
[41]M. E. Barone and D. B. Graves, J. Appl. Phys. **77**, 1263 (1995).
[42]M. Balooch, M. Moalem, W. E. Wang, and A. V. Hamza, J. Vac. Sci. Technol. A **14**, 229 (1996).
[43]J. P. Chang and H. H. Sawin, J. Vac. Sci. Technol. A **15**, 610 (1997).
[44]F. Gou, M. A. Gleeson, and A. W. Kleyn, Phys. Chem. Chem. Phys. **8**, 5522 (2006).
[45]I. P. Herman, V. M. Donnelly, C. C. Cheng, and K. V. Guinn, Jpn. J. Appl. Phys., Part 1 **35**, 2410 (1996).